air for 30 min at 450°C and (ii) refluxing in 4 M HCl at 120°C for 24 hours.
11. H. E. Romero, G. U. Sumanasekera, G. D. Mahan, P. C. Eklund, *Phys. Rev. B* **65**, 205410 (2002).
12. P. G. Collins, K. Bradley, M. Ishigami, A. Zettl, *Science* **287**, 1801 (2000).
13. G. U. Sumanasekera *et al.*, *Phys. Rev. B* **65**, 035408 (2001).
14. We have observed a sample-dependent difference in S_0 that depends on the nature and quality of the purification process. The value depends, for example, on whether HNO_3 or HCl is used to remove residual catalyst from the material. Care must be taken to degas the purified material at ~200°C in a high vacuum (i.e., better than $\sim 10^{-6}$ torr) for 10 to 24 hours and to directly observe the asymptotic approach of S to S_0. In our measurements on about 100 samples mostly derived from electric ARC–produced material, we find that samples with the lowest amorphous carbon content and residual metal catalyst show the smallest, negative S_0 value (i.e., $S_0 \sim -3$ to -8 V/K). The "best" samples had D-band Raman scattering intensity ~1/20 (or less) than that of the T-band scattering, and had measured metal content of ~0.1 to ~0.5 weight % (wt %). Some samples exhibited S_0 as large as −50 V/K. Despite this variation in S_0, all samples that reached an asymptotic negative TEP value to S_0 in the range from −3 to −50 V/K showed essentially the same characteristic response of the transport parameters (R, S) to a specific gas.
15. R. D. Barnard, *Thermoelectricity in Metals and Alloys* (Taylor and Francis, London, 1972).
16. Recently, a broad peak in $S(T)$, observed below 100 K and superimposed on a linear T background, has been attributed to an additional contribution from phonon drag (*11*, *17*). Because our measurements in this study were made at 500 K, we ignore a phonon drag contribution that is a low-temperature effect.
17. J. Vavro *et al.*, *Phys. Rev. Lett.* **90**, 065503 (2003).
18. This assumption is an application of Matthiessen's rule (*15*).
19. H. E. Romero, P. C. Eklund, unpublished data.
20. P. B. Allen, in *Superconductivity in D- and F-Band Metals*, H. Suhl, M. B. Maple, Eds. (Academic Press, New York, 1980).
21. P. L. Rossiter, *The Electrical Resistivity of Metals and Alloys* (Cambridge Univ. Press, Cambridge, 1987).
22. K. Bolton, A. Rosen, *Phys. Chem. Chem. Phys.* **4**, 4481 (2002).
23. The (10,0) tube is semiconducting and has a diameter of 7.83 Å. It is sufficiently small to facilitate the simulation of a large number of scattering events required for statistical analysis.
24. This was done by scaling the velocity of the carbon atoms at the tube ends to zero at each trajectory time step. In this way, energy flowing in the tube axial direction was adsorbed, but not energy that flows in the tube radial or circumferential directions.
25. Saito *et al.* (*2*) reported on the strong diameter dependence of the squash mode. By using their calculated squash-mode frequency for a (10,10) tube, we estimate that the squash-mode frequency for a (10,0) tube is 29 cm^{-1}. In our molecular simulations we observe 43 cm^{-1}. The short length of the nanotube which is clamped at the ends may upshift the squash-mode frequency relative to that obtained for an infinite tube.
26. We also found that the slopes of theoretical lines of the average tube energy and the maximum radial displacement as a function of the colliding mass decrease with time.
27. J.-Q. Lu *et al.*, *Phys. Rev. Lett.* **90**, 156601/1 (2003).
28. C.-J. Park, Y.-H. Kim, K. J. Chang, *Phys. Rev. B* **60**, 10656 (1999).
29. The authors gratefully acknowledge many helpful discussions with G. D. Mahan. This work was supported by NSF (P.C.E.), Pennsylvania State University (P.C.E. and H.R.), and the Swedish Foundation for Strategic Research (A.R. and K.B.).

25 June 2004; accepted 1 December 2004
10.1126/science.1102004

Observation of Large Water-Cluster Anions with Surface-Bound Excess Electrons

J. R. R. Verlet,[1] A. E. Bragg,[1] A. Kammrath,[1] O. Cheshnovsky,[2] D. M. Neumark[1,3]*

Anionic water clusters have long been studied to infer properties of the bulk hydrated electron. We used photoelectron imaging to characterize a class of $(H_2O)_n^-$ and $(D_2O)_n^-$ cluster anions ($n \leq 200$ molecules) with vertical binding energies that are significantly lower than those previously recorded. The data are consistent with a structure in which the excess electron is bound to the surface of the cluster. This result implies that the excess electron in previously observed water-cluster anions, with higher vertical binding energies, was internally solvated. Thus, the properties of those clusters could be extrapolated to those of the bulk hydrated electron.

The hydrated electron (*1*), which is localized and supported within a cavity formed by surrounding water molecules, plays a prominent role in many areas of condensed-phase science such as radiation physics, biological activity, electron transfer, and charge-induced reactivity. Gas-phase clusters of solvent molecules have also been observed to carry an extra charge (*2*), and they represent microscopic analogs to their bulk counterparts, assuming that sufficient solvent molecules are present. For water clusters, however, the critical size beyond which the cluster anion resembles the bulk hydrated electron has remained a controversial issue. Specifically, there are believed to be two localization modes for an excess electron in a water cluster: an internally solvated electron, akin to the bulk; and an electron localized on the surface of the cluster (*3*).

Significant theoretical effort has been devoted to understanding the nature of the excess electron in water clusters, $(H_2O)_n^-$. Path-integral molecular dynamics simulations found that surface states are more stable at sizes up to $n = 32$ molecules, whereas the internal electron is more stable for $n \geq 64$ (*3*). Electron vertical binding energies (VBEs), which correspond to the minimum amount of energy required to remove the electron from the cluster anion with no molecular rearrangement, were predicted to be considerably lower for the surface states than for the internal states. Thus, photoelectron (PE) spectroscopy of $(H_2O)_n^-$ clusters should yield the size at which the surface-to-internal structural transformation occurs.

However, PE spectra measured by Coe *et al.* (*4*) showed no evidence for a surface-to-internal transition in the predicted size range. Instead, the measured VBEs from $(H_2O)_{11}^-$ up to $(H_2O)_{69}^-$ scaled linearly with the inverse of the cluster radius or, equivalently, as $n^{-1/3}$. Such a correlation is expected for an internally solvated electron within a simple dielectric model (*5*), which recovers the observed gradient using the known dielectric constants of bulk water (*4*, *6*). Furthermore, extrapolation of the VBE to infinite size (the bulk) yielded a value of 3.3 eV, which is close to the photoelectric threshold of water, 3.2 eV, estimated by Coe *et al.* (*4*). This result supports the idea that there is an internally solvated electron in these clusters. However, the measured VBEs are in good agreement with VBEs calculated for surface states (*3*), providing the alternative interpretation that surface states were observed in the experiments. There is a similar inconsistency in the electronic absorption spectra of $(H_2O)_n^-$ ($15 \leq n \leq 50$) (*7*), in which the maxima also scale linearly with $n^{-1/3}$ and extrapolate to the observable bulk value (*1*). But, those spectra were also found to be in agreement with the calculated values for surface rather than internal states (*8*). Finally, even though PE spectra of $I^-(H_2O)_n$ clusters showed a VBE-versus-$n^{-1/3}$ correlation with the same gradient as $(H_2O)_n^-$ clusters (*9*), there is consensus that the iodide resides on the surface of small- to medium-sized clusters (*10*, *11*).

The issue of internal versus surface structures has reemerged in the context of two recent time-resolved PE spectroscopy studies focusing on the dynamics of $(H_2O)_n^-$ clusters after electronic excitation (*12*, *13*). Measurement of the internal conversion lifetime of $(H_2O)_n^-$ as a function of size ($n = 25$ to 50) extrapolated to a bulk value of 50 fs, supporting a nonadiabatic

[1]Department of Chemistry, University of California, Berkeley, CA 94720, USA. [2]School of Chemistry, The Sacker Faculty of Exact Sciences, Tel-Aviv University, 69978, Israel. [3]Chemical Science Division, Lawrence Berkeley National Laboratory, Berkeley, CA 94720, USA.

*To whom correspondence should be addressed. E-mail: dneumark@berkeley.edu

relaxation model for the bulk hydrated electron (*14*). However, extrapolations to the bulk assume that cluster anions are akin to the hydrated electron. Without direct evidence, the question of electron localization in $(H_2O)_n^-$ clusters has remained open.

The nature of electron binding in water-cluster anions can be clarified by locating $(H_2O)_n^-$ isomers with either higher or lower VBEs in the size range studied by Coe *et al.* (*4*). Here, we report observation of a class of water-cluster anions with significantly lower VBEs than those previously reported and assign them to clusters with surface-bound electrons. These clusters were generated by means of a new pulsed valve (*15*) capable of producing very cold molecular beam conditions, and the clusters were characterized using one-photon and time-resolved PE imaging.

Our PE imaging apparatus has been described in detail elsewhere (*16*). Clusters were generated by passing Ar-carrier gas over water (H_2O or D_2O) at 20°C and were injected into the vacuum chamber by means of an Even-Lavie pulsed valve, operated at 100 Hz (*15*). The gas mixture was crossed by high-energy electrons (~500 eV), generating anions through secondary-electron attachment near the throat of the expansion. Anion clusters were then extracted and mass-selected by their time of flight before the laser interaction. Electrons were detached from the cluster by a ~100-fs laser pulse centered at a wavelength of 398 nm ($h\nu$ = 3.11 eV, where h is Planck's constant and ν is the frequency of the laser pulse). The ejected PEs were analyzed by velocity-map imaging (*17*), in which an electrostatic lens projected the three-dimensional (3D) PE velocity distribution onto a focal plane. On this focal plane, a 70-mm multichannel-plate detector coupled to a phosphor screen provided a visual display of the emitted electron cloud, and we captured these images on a charge-coupled device (CCD) camera. PE spectra were then reconstructed from the 2D images using standard methods (*18*).

The one-photon experiments revealed the existence of water-cluster anion isomers with low VBEs. The dynamics of these isomers were characterized by pump-probe experiments, in which an initial pulse of ~100 fs duration and centered at a wavelength of 1650 nm (0.75 eV) pumped the population into an excited state, which was then probed with a delayed probe pulse at a wavelength of 790 nm and of similar time duration.

We acquired PE spectra of a number of $(H_2O)_n^-$ and $(D_2O)_n^-$ clusters, where n = 11 to 200. The effect of varying source backing pressure is shown for $(D_2O)_{50}^-$ in Fig. 1. The black line shows a typical PE spectrum with VBE = 1.78 eV, in agreement with the results of Coe *et al.* (*4*). By gradually increasing the source backing pressure, which generally correlates to cooling of the cluster ensemble, we observed a new feature at lower VBE. At a backing pressure of 70 pounds per square inch (psi), this feature dominates the PE spectrum, and it has a maximum at VBE = 0.97 eV. This observed transition confirms the presence of two distinct species in the molecular beam, labeled as isomers I and II.

A series of PE spectra for $(D_2O)_n^-$ with n = 11 to 150 was collected both at low (30 psi) and high (70 psi) backing pressures (Fig. 2). For clusters with $n > 50$, the PE spectra taken at higher pressure have a single broad asymmetric feature, attributed solely to isomer II. For $n < 50$, isomer I cannot be completely removed in the pressure range studied (30 to 70 psi), and its PE signature increases relative to isomer II as the size is decreased. For these smaller clusters, an additional feature was observed at very small VBE indicated by asterisks in Fig. 2 (isomer III). PE spectra for $(H_2O)_n^-$ are similar to those of $(D_2O)_n^-$ for sizes $n > 50$. Smaller clusters of $(H_2O)_n^-$ do not appear to form isomer II and III as readily, and neither isomer was observed below n = 27.

In Fig. 3, we compare the VBEs of these differing isomers with previously reported VBEs and their $n^{-1/3}$ dependence (*4*, *19*). Our measurements for isomer I are in agreement with those obtained by Coe *et al.* (*4*). Isomer II clusters show consistently smaller VBEs than isomer I clusters, and they scale linearly with $n^{-1/3}$ for $11 \le n \le 20$ and for $n > 50$, with a steeper slope for the set of larger clusters. The VBEs for both isomers II and III appear to connect smoothly, toward smaller sizes, with those previously reported by Kim *et al.* (*19*), who observed two isomers for several $(H_2O)_n^-$ clusters with $n \le 11$. Figure 3 also includes results from molecular dynamics simulations (*3*), illustrating the apparent agreement of the calculated surface VBEs with isomer I.

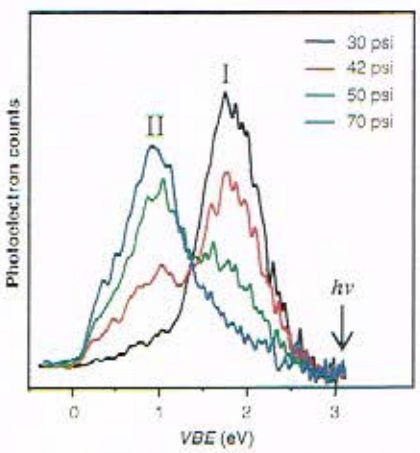

Fig. 1. PE spectra of $(D_2O)_{50}^-$ under varying cluster source conditions. The peaks assigned to internally solvated and surface-localized electron isomers are labeled as I and II, respectively. Different line colors represent PE spectra taken at various backing pressures.

The observation of different isomers over a large range of cluster sizes suggests differing modes of electron localization. Theoretical studies find that the isomer with a lower VBE has its electron localized near the surface of the cluster (*3*), which leads us to assign isomer II to surface states; isomer I is assigned to clusters with internalized electrons. Scaling the VBEs that were calculated from molecular dynamics simulations by 60% for both surface and internal states yielded good agreement with the experimental VBEs for isomers II and I, respectively (Fig. 3). This result implies too strong an electron-water interaction in the model potential used to calculate the VBEs (*20*). The assignment of isomer I to clusters with an internally localized electron agrees with the original assignment by Coe *et al.* (*4*) and validates our extrapolation of the excited-state dynamics in $(H_2O)_n^-$ clusters to those of the bulk hydrated electron (*12*).

Time-resolved pump-probe experiments provided further characterization of isomer II.

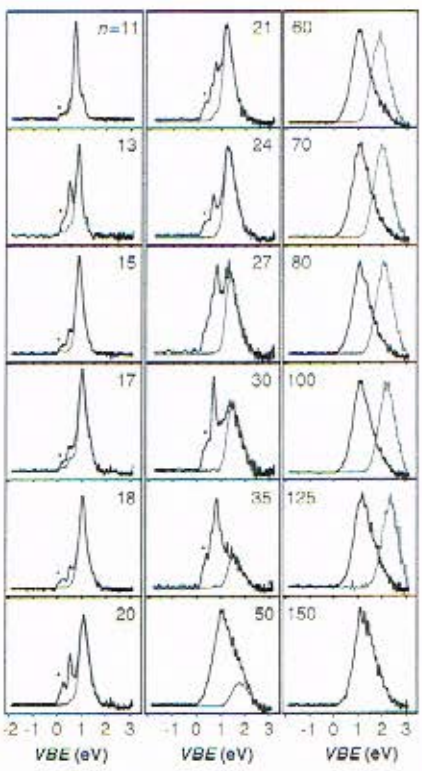

Fig. 2. PE spectra of $(D_2O)_n^-$ with $11 \le n \le 150$ at 30 psi (gray) and 70 psi (black). The peaks marked with asterisks show the presence of a second surface state, isomer III. For n = 11 to 50, the PE feature caused by the internally solvated isomer (gray) is scaled to highlight its contribution to the total PE spectra collected at 70 psi. For n = 60 to 125, there is virtually no contribution from the internally solvated isomer, and the PE spectra for these are scaled to the intensity of the PE spectra from the surface-bound isomer.

In particular, clusters with surface-bound electrons were predicted to support excited states (*8*), and their relaxation rates may thus be quantified by measuring the PE signal at highest electron kinetic energy, corresponding to the time-dependent pump-probe signal (*21*). We measured excited-state lifetimes for $(H_2O)_n^-$ and $(D_2O)_n^-$ clusters with $60 \leq n \leq 100$ under conditions where only isomer II was present, and compared them to those previously obtained for isomer I (Fig. 4) (*12*). The lifetimes for isomer II were longer and were nearly size-independent. This size invariance suggests a significantly weaker coupling of the electron to the solvent network, compared to the $1/n$ dependence observed for isomer I clusters (*12*). The results in Fig. 4 reinforce our assignments of isomers I and II, because a surface-bound excess electron is expected to be less strongly coupled to the solvent network than an internally localized electron.

The VBEs measured for isomer II of $(D_2O)_n^-$ with $11 \leq n \leq 20$ merge with those measured by Coe *et al.* (*4*) and Kim *et al.* (*19*) for $(H_2O)_n^-$ with $n \leq 11$. This suggests a common structural motif in the two size ranges. Recent theoretical and experimental work (*22*–*24*) indicates that for clusters with $n \leq 7$, the lowest energy anion structure is one where a double hydrogen-bond accepting (AA) water molecule acts as the binding site for the excess electron. The electron is bound by a combination of high dipole moment of the overall solvent network and, more locally, by the two dangling H atoms from the AA water. Our results support a similar electron-binding scheme for isomer II with $11 \leq n \leq 20$. The evolution of isomer II VBEs for larger cluster sizes, however, suggests a transitional region for $20 < n < 50$, as a new electron-binding motif is established for $n > 50$, characterized by stronger binding and a more pronounced dependence on cluster radius. Only at these large cluster sizes does the surface-bound motif for $(H_2O)_n^-$ clusters become prominent at colder conditions, providing further evidence for a qualitative change in the electron binding once this size is reached. The nature of electron binding to clusters with $n > 50$ is likely to be similar to those observed in simulations (*3*). A local environment involving single acceptor H atoms from a small number of solvent molecules binds the electron on the cluster surface. The electron is further stabilized by the long-range polarization energy induced in the solvent network. The latter effect is demonstrated by the larger gradient in the VBE versus $n^{-1/3}$ plot.

Analogous arguments suggest that isomer III, seen for $(D_2O)_n^-$ with $11 \leq n \leq 35$, may have similar electron-binding motifs to the lower-VBE isomers observed by Kim *et al.* for $(H_2O)_n^-$ with $n \leq 11$ (*19*). By measuring photodetachment cross-sections of the two isomers of $(H_2O)_6^-$, Bailey and Johnson concluded that the electron distribution for the lower-VBE isomer is significantly more diffuse (*25*). This conclusion is supported by ab initio calculations (*23*), predicting a hook-like solvent structure for the lower VBE isomer for which the dipole moment of 5.5 D is about half that of the $(H_2O)_6$ structure with the AA water molecule. The evolution of the isomer III VBEs thus suggests a more diffuse surface-electron bound by a number of dangling H atoms. The very weak size dependence of this isomer also suggests that the collective network provides little stabilization because the electron is delocalized over much of the surface.

Regarding the mechanism by which the differing isomers are formed, the considerably higher VBEs for isomer I indicate that it is the more stable anion for $n > 11$. However, isomers II and III are favored by higher source backing pressure, which is generally associated with forming colder and more stable clusters. It appears that isomers II and III are metastable species whose formation is enhanced under colder expansion conditions. These results can be rationalized, given that water-cluster anions are most likely formed in the pulsed jet by the attachment of relatively low-energy electrons to neutral clusters, which then continue to grow as the expansion progresses. As the backing pressure increases, the neutral clusters should be larger and colder in the region of expansion where electron attachment occurs. Hence, under normal conditions similar to those used by Coe *et al.* (*4*) (30 psi in our experiment), we propose that the electrons are attaching to relatively warm, liquid-like clusters, and further solvent molecules may condense onto the cluster after attachment. Furthermore, solvent rearrangement to form the lowest energy anion configuration occurs readily because of the high internal energy available in the solvent network. On the other hand, formation of large anions with surface-localized electrons occurs under much colder conditions, where a small local reorganization can bind the electron on the surface, but the overall low internal energy inhibits the large solvent reorganization necessary to form the internally solvated electron. In that sense, the binding process of the large clusters ($n > 50$) may be viewed as electron attachment to an ice nanocrystal.

For smaller clusters, where $11 \leq n \leq 20$, the situation is less clear. No neutral $(H_2O)_n$ clusters with AA water molecules have been observed experimentally (*26*). Assuming that the isomer II cluster anions involve an electron binding to an AA water molecule, it appears that these species cannot be formed by simply adding an electron to a neutral cluster; a substantial amount of solvent rearrangement is

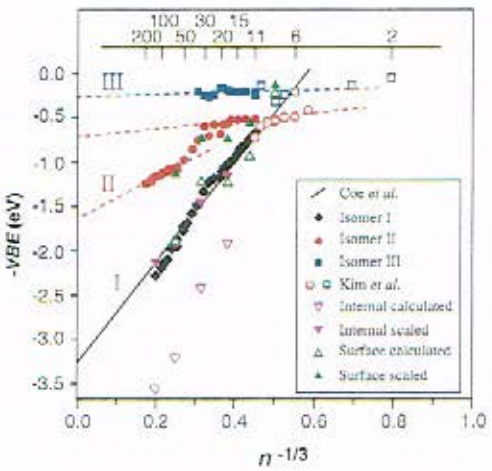

Fig. 3. Plots of VBEs for water-cluster anions versus $n^{-1/3}$. VBEs for isomer I were obtained under conditions similar to those used in previous studies. VBEs for isomers II and III of $(D_2O)_n^-$ were extracted from Fig. 2. Isomer II data also include VBEs obtained for $(H_2O)_n^-$ with $60 \leq n \leq 200$. The linear fit to data from Coe *et al.* is taken from (*6*). Data from Kim *et al.* (*19*) for clusters with $n \leq 11$ are also shown. Data labeled "internal calculated" and "surface calculated" are from molecular dynamics (MD) simulations (*3*); also shown are MD binding energies scaled by 60%.

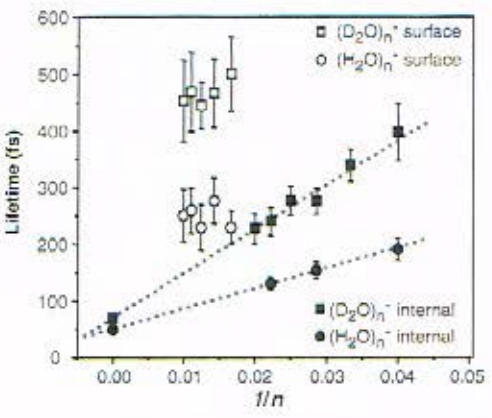

Fig. 4. Pump-probe results for surface and internal states. Relaxation time scales are given after electronic excitation of the surface isomers at 0.75 eV (open symbols) and internal isomers at 1.0 eV (solid symbols) of $(H_2O)_n^-$ (circles) and $(D_2O)_n^-$ (squares). Relaxation dynamics of the internal states follow a $1/n$ size dependence (*12*), whereas dynamics of the surface states are slower and show no size dependence.

required even for a surface state. The observation of isomer II clusters in this size range only for $(D_2O)_n^-$ attests to the fragility of these isomers. They are most likely associated with shallow local minima on the overall potential energy landscape and exist only because of the lower zero-point energies and tunneling rates associated with D_2O as compared to H_2O (*27*). These considerations may explain why, even for larger clusters where we see isomers I and II for both isotopomers, it is easier to make the surface-bound isomer II for $(D_2O)_n^-$ clusters. The preference for isomer I in $(H_2O)_n^-$ clusters could also be a manifestation of the greater stability of the hydrated electron in liquid H_2O than in D_2O (*28*).

References and Notes

1. E. J. Hart, J. W. Boag, *J. Am. Chem. Soc.* **84**, 4090 (1962).
2. H. Haberland, C. Ludewight, H. G. Schindler, D. R. Worsnop, *J. Chem. Phys.* **81**, 3742 (1984).
3. R. N. Barnett, U. Landman, C. L. Cleveland, J. Jortner, *J. Chem. Phys.* **88**, 4429 (1988).
4. J. V. Coe *et al.*, *J. Chem. Phys.* **92**, 3980 (1990).
5. R. N. Barnett, U. Landman, C. L. Cleveland, J. Jortner, *Chem. Phys. Lett.* **145**, 382 (1988).
6. J. V. Coe, *Int. Rev. Phys. Chem.* **20**, 33 (2001).
7. P. Ayotte, M. A. Johnson, *J. Chem. Phys.* **106**, 811 (1997).
8. R. N. Barnett, U. Landman, G. Makov, A. Nitzan, *J. Chem. Phys.* **93**, 6226 (1990).
9. G. Markovich, S. Pollack, R. Giniger, O. Cheshnovsky, *J. Chem. Phys.* **101**, 9344 (1994).
10. W. H. Robertson, M. A. Johnson, *Annu. Rev. Phys. Chem.* **54**, 173 (2003).
11. P. Jungwirth, D. J. Tobias, *J. Phys. Chem. B* **106**, 6361 (2002).
12. A. E. Bragg, J. R. R. Verlet, A. Kammrath, O. Cheshnovsky, D. M. Neumark, *Science* **306**, 669 (2004).
13. D. H. Paik, I.-R. Lee, D. S. Yang, J. S. Baskin, A. H. Zewail, *Science* **306**, 672 (2004).
14. M. S. Pshenichnikov, A. Baltuska, D. A. Wiersma, *Chem. Phys. Lett.* **389**, 171 (2004).
15. U. Even, J. Jortner, D. Noy, N. Lavie, C. Cossart-Magos, *J. Chem. Phys.* **112**, 8068 (2000).
16. A. E. Bragg, J. R. R. Verlet, A. Kammrath, O. M. Neumark, *J. Chem. Phys.* **121**, 3515 (2004).
17. A. T. J. B. Eppink, D. H. Parker, *Rev. Sci. Instrum.* **68**, 3477 (1997).
18. V. Dribinski, A. Ossadtchi, V. A. Mandelshtam, H. Reisler, *Rev. Sci. Instrum.* **73**, 2634 (2002).
19. J. Kim, I. Becker, O. Cheshnovsky, M. A. Johnson, *Chem. Phys. Lett.* **297**, 90 (1998).
20. D. M. Bartels, *J. Chem. Phys.* **115**, 4404 (2001).
21. A. E. Bragg, J. R. R. Verlet, A. Kammrath, O. Cheshnovsky, D. M. Neumark, unpublished data.
22. H. M. Lee, S. B. Suh, K. S. Kim, *J. Chem. Phys.* **118**, 9981 (2003).
23. H. M. Lee, S. Lee, K. S. Kim, *J. Chem. Phys.* **119**, 187 (2003).
24. N. I. Hammer *et al.*, *Science* **306**, 675 (2004).
25. C. G. Bailey, M. A. Johnson, *Chem. Phys. Lett.* **265**, 185 (1997).
26. U. Buck, F. Huisken, *Chem. Rev.* **101**, 205 (2001).
27. F. N. Keutsch, R. J. Saykally, *Proc. Natl. Acad. Sci. U.S.A.* **98**, 10533 (2001).
28. P. Han, D. M. Bartels, *J. Phys. Chem.* **95**, 5367 (1991).

29. This research is supported by NSF grant no. CHE-0350585. Additional support from the United States–Israel Binational Science Foundation is gratefully acknowledged.

25 October 2004; accepted 22 November 2004
Published online 16 December 2004;
10.1126/science.1106719
Include this information when citing this paper.

Liquid Crystalline Networks Composed of Pentagonal, Square, and Triangular Cylinders

Bin Chen,[1] Xiangbing Zeng,[3] Ute Baumeister,[2] Goran Ungar,[3] Carsten Tschierske[1]*

T-shaped molecules are designed in such a way that they self-organize into nanoscale liquid crystalline honeycombs based on polygons with any chosen number of sides. One of the phases reported here is a periodic organization of identical pentagonal cylinders; the other one is a structure composed of square-shaped and triangular cylinders in the ratio 2:1. These two different packing motifs represent duals of the same topological class. The generalization of the concept applied here allows the prediction of a whole range of unusual complex liquid crystalline phases.

One of the fascinating aspects of beehive honeycombs is their nearly perfect hexagonal structure. Although it is intuitively "obvious" that this is the way to pack cylinders with the minimum wall area, the mathematical proof came only recently (*1*). Whether we look at living tissue or the organization of nanoparticles, molecules, or atoms, one can find numerous examples of hexagonal patterns. The situation is different for pentagons. In contrast to hexagons, regular pentagons, whose edge lengths and angles are all equal, fail to tile the plane, a fact that has intrigued humans since ancient times (*2*, *3*). However, snugly fitting pentagons can tile the sphere, either by themselves (pentagonal dodecahedron) or in combination with hexagons [e.g., fullerenes (*4*) or supermolecules like polyoxometallates (*5*)]. In contrast, tiling of a flat plane by identical pentagons can be achieved only if regular pentagons are mixed with other polygons in a nonperiodic arrangement [Penrose tilings (*6*, *7*)] or if they contain at least two different angles and side lengths (*8*, *9*). The latter is difficult to realize on a molecular scale with the rather strongly fixed angles and distances dictated by covalent bonding and coordination of standard chemical building blocks. Hence, only a nonplanar two-dimensional (2D) net of pentagons has been realized with a coordination polymer (*10*). We show that the liquid crystalline state (*11*), which combines order and mobility, provides the necessary degree of flexibility for the realization of pentagonal honeycombs.

Liquid crystals (LCs) are known as materials for flat, low power–consuming displays in computing and telecommunication devices. The self-organization within the liquid crystalline phases is driven by the molecular shape, leading to long-range orientational order, and by

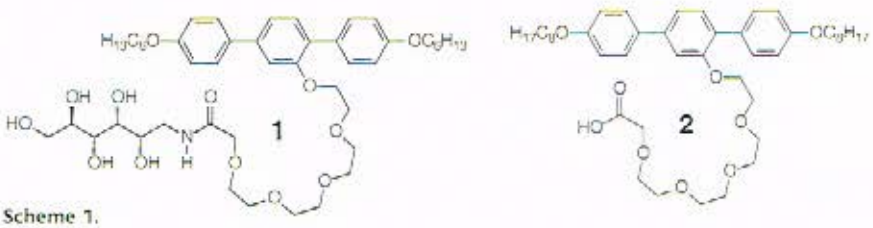

Scheme 1.

Table 1. Phase transition temperatures (*T*) of compounds 1 and 2 (*18*) and the volume fractions of polar side chains (f_s) and nonpolar end chains (f_e). Abbreviations: Cr, crystalline solid state; $Col_{squ}/p4gm$, square columnar phase of the plane group *p4gm*; $Col_{squ}/p4mm$, square columnar phase of the plane group *p4mm*; $Col_{hex}/p6mm$, hexagonal columnar phase of the plane group *p6mm*; Iso, isotropic liquid state.

Compound	*T* (°C)	f_s	f_e
1	Cr 50 $Col_{squ}/p4gm$ 105 $Col_{hex}/p6mm$ 118 Iso	0.29	0.44
2	Cr 21 $Col_{squ}/p4gm$ 30 $Col_{squ}/p4mm$ 31 Iso	0.41	0.30

[1]Institute of Organic Chemistry, [2]Institute of Physical Chemistry, Martin-Luther-University Halle-Wittenberg, Kurt-Mothes-Strasse 2, D-06120 Halle, Germany. [3]Department of Engineering Materials and Centre for Molecular Materials, University of Sheffield, Sheffield S1 3JD, UK.

*To whom correspondence should be addressed. E-mail: carsten.tschierske@chemie.uni-halle.de

Observation of Large Water-Cluster Anions with Surface-Bound Excess Electrons

J. R. R. Verlet,[1] A. E. Bragg,[1] A. Kammrath,[1] O. Cheshnovsky,[2] D. M. Neumark[1,3]*

Anionic water clusters have long been studied to infer properties of the bulk hydrated electron. We used photoelectron imaging to characterize a class of $(H_2O)_n^-$ and $(D_2O)_n^-$ cluster anions ($n \leq 200$ molecules) with vertical binding energies that are significantly lower than those previously recorded. The data are consistent with a structure in which the excess electron is bound to the surface of the cluster. This result implies that the excess electron in previously observed water-cluster anions, with higher vertical binding energies, was internally solvated. Thus, the properties of those clusters could be extrapolated to those of the bulk hydrated electron.

The hydrated electron (1), which is localized and supported within a cavity formed by surrounding water molecules, plays a prominent role in many areas of condensed-phase science such as radiation physics, biological activity, electron transfer, and charge-induced reactivity. Gas-phase clusters of solvent molecules have also been observed to carry an extra charge (2), and they represent microscopic analogs to their bulk counterparts, assuming that sufficient solvent molecules are present. For water clusters, however, the critical size beyond which the cluster anion resembles the bulk hydrated electron has remained a controversial issue. Specifically, there are believed to be two localization modes for an excess electron in a water cluster: an internally solvated electron, akin to the bulk; and an electron localized on the surface of the cluster (3).

Significant theoretical effort has been devoted to understanding the nature of the excess electron in water clusters, $(H_2O)_n^-$. Path-integral molecular dynamics simulations found that surface states are more stable at sizes up to $n = 32$ molecules, whereas the internal electron is more stable for $n \geq 64$ (3). Electron vertical binding energies (VBEs), which correspond to the minimum amount of energy required to remove the electron from the cluster anion with no molecular rearrangement, were predicted to be considerably lower for the surface states than for the internal states. Thus, photoelectron (PE) spectroscopy of $(H_2O)_n^-$ clusters should yield the size at which the surface-to-internal structural transformation occurs.

[1]Department of Chemistry, University of California, Berkeley, CA 94720, USA. [2]School of Chemistry, The Sackler Faculty of Exact Sciences, Tel-Aviv University, 69978, Israel. [3]Chemical Sciences Division, Lawrence Berkeley National Laboratory, Berkeley, CA 94720, USA.
*To whom correspondence should be addressed. E-mail: dneumark@berkeley.edu

www.sciencemag.org SCIENCE VOL 307 7 JANUAR

"Specifically, there are believed to be two localization modes for an excess electron in a water cluster: an internally solvated electron, akin to the bulk; and an electron localized on the surface of the cluster (3).

(中略)

Path-integral molecular dynamics simulations found that surface states are more stable at sizes up to n = 32 molecules, whereas the internal electron is more stable for n ≥ 64 (3)."

中でも、水のクラスター内に存在する余剰電子には２つの局在様式があると考えられている。一つはバルク溶媒和電子のようにクラスター内で溶媒和された電子。もう一つはクラスターの表面に局在する電子である（3)。

(中略)

経路積分分子動力学のシミュレーションにより、水分子数が最大で n=32 個の場合には電子が（クラスターの）表面にある方が安定し、一方で水分子数が n≧64 の場合には電子が（クラスターの）内部に局在した方が安定することが明らかとなった（3)。